Synaptopodin-deficient mice lack a spine apparatus and show deficits in synaptic plasticity

Thomas Deller[a,b,c], Martin Korte[c,d], Sophie Chabanis[c,e,f], Alexander Drakew[a], Herbert Schwegler[g], Giulia Good Stefani[d], Aimee Zuniga[e,h], Karin Schwarz[i], Tobias Bonhoeffer[d], Rolf Zeller[e,h,j], Michael Frotscher[a,j,k], and Peter Mundel[f,i,j,l]

[a]Institute of Anatomy, University of Freiburg, P.O. Box 111, D-79001 Freiburg, Germany; [b]Institute of Clinical Neuroanatomy, University of Frankfurt, Theodor-Stern-Kai 7, D-60590 Frankfurt, Germany; [d]Department of Cellular and Systems Neurobiology, Max Planck Institute of Neurobiology, D-82152 Martinsried, Germany; [e]European Molecular Biology Laboratory, Meyerhofstrasse 1, D-69117 Heidelberg, Germany; [f]Department of Anatomy and Cell Biology, University of Heidelberg, Im Neuenheimer Feld 307, D-69120 Heidelberg; [g]Institute of Anatomy, University of Magdeburg, Leipzigerstrasse 44, D-39120 Magdeburg, Germany; [h]Department of Developmental Biology, Faculty of Biology, Utrecht University, Padualaan 8, NL-3584CH Utrecht, The Netherlands; and [i]Department of Medicine and Department of Anatomy and Structural Biology, Albert Einstein College of Medicine, 1300 Morris Park Avenue, Bronx, NY 10461

Edited by Hans Thoenen, Max Planck Institute of Neurobiology, Martinsried, Germany, and approved July 9, 2003 (received for review April 22, 2003)

The spine apparatus is a cellular organelle that is present in many dendritic spines of excitatory neurons in the mammalian forebrain. Despite its discovery >40 years ago, the function of the spine apparatus is still unknown although calcium buffering functions as well as roles in synaptic plasticity have been proposed. We have recently shown that the 100-kDa protein synaptopodin is associated with the spine apparatus. Here, we now report that mice homozygous for a targeted deletion of the *synaptopodin* gene completely lack spine apparatuses. Interestingly, this absence of the spine apparatus is accompanied by a reduction in hippocampal long-term potentiation (LTP) in the CA1 region of the hippocampus and by an impairment of spatial learning in the radial arm maze test. This genetic analysis points to a role of the spine apparatus in synaptic plasticity.

Dendrites of many neurons are covered with small appendages or "spines" that contain the postsynaptic elements for the contact of the respective dendrite with excitatory afferents (1). Spines form biochemical microcompartments largely separated from the parent dendrite (2, 3) and they have been hypothesized to be sites of synaptic plasticity in the brain (2, 4–9). Their number, shape, and size depend on various factors such as neuronal activity and hormonal and environmental stimuli (10–17). Many telencephalic spines contain a distinct organelle, the spine apparatus, that consists of stacks of smooth endoplasmic reticulum (sER) interdigitated by electron-dense plates (1, 18, 19). The function of the spine apparatus in synaptic transmission is largely unknown although a role in local calcium storage has been postulated (20, 21). This in turn suggests a possible role of the spine apparatus in synaptic plasticity, because release of calcium from internal stores is known to be involved in activity-dependent synaptic plasticity (2, 22–25).

We have recently shown that Synaptopodin, a 100-kDa proline-rich protein (26), is closely associated with the spine apparatus in spines of telencephalic neurons (27). In adult mice, *synaptopodin* transcripts are expressed in the olfactory bulb, cerebral cortex, striatum, and hippocampus, but not in the cerebellum. In addition, Synaptopodin is also expressed in podocytes of kidney glomeruli (26). The tight association of Synaptopodin with the spine apparatus suggested that Synaptopodin is an important component of this organelle (27, 28). We therefore generated *synaptopodin*-deficient mice by gene-targeting and assessed the morphological and functional consequences of the Synaptopodin deficiency. Mice developed normally and did not show pathohistological changes. The number and length of dendritic spines on cortical neurons were normal. However, we discovered that spine apparatuses were completely absent in *synaptopodin*-deficient mice. In view of the postulated function of the spine apparatus in synaptic plasticity, we studied synaptic plasticity in adult mice lacking Synaptopodin function.

Methods

Inactivation of *synaptopodin* by Gene Targeting. The *synaptopodin* gene was cloned from a genomic bacterial artificial chromosome (BAC) library (Genome Systems, St. Louis) and inactivated by homologous recombination in embryonic stem (ES) cells (E14/129/Ola). The targeting construct was made in a classical replacement vector termed pHM2 (29) with modifications. To ensure that a null allele was generated, the coding region was replaced by the *lacZ* gene, which was fused in frame downstream of the ATG (Fig. 1*A*). The selectable *neomycin* resistance marker was flanked by LoxP sites and inserted downstream of the *lacZ* gene. Screening of ES cell clones for homologous recombination was performed by Southern blot analysis (Fig. 1*B*). A total of 151 ES cell clones were screened, and 12 positive clones were obtained. Two of these clones were injected into blastocysts and germ-line transmission was obtained. Heterozygous animals were intercrossed to generate homozygous mice. Genotyping was performed by PCR and the line was maintained in a 129/C57BL6 (F_1) mixed genetic background. All analyses were performed with the investigator blind to genotype.

Electron Microscopy. Wild-type (male; $n = 5$) and mutant mice (male; $n = 5$) were deeply anesthetized with an overdose of Nembutal (300 mg/kg body weight) and were fixed by transcardial perfusion as described (27). Experiments were performed in agreement with the German law on the use of laboratory animals. Frontal sections (50 μm) of neocortex, striatum, and hippocampus were embedded and serially thin-sectioned for electron microscopy (27, 28).

Synaptopodin Immunostaining. Frontal sections of hippocampus, neocortex and striatum (50 μm) from wild-type and mutant mice (male and female; $n = 8$ for each genotype), were immunostained with rabbit anti-Synaptopodin (26) and processed for light and electron microscopy (27). Some sections were used for preembedding immunogold labeling (grain size: 1.4 nm). In control experiments, the primary antibody was omitted. No immunostaining was observed in *synaptopodin* mutant mice (Fig. 2 *A* and *B*).

Quantification of Spine Apparatuses. In random ultrathin sections of neocortex, striatum, and hippocampus (stratum radiatum of

This paper was submitted directly (Track II) to the PNAS office.

Abbreviations: sER, smooth endoplasmic reticulum; ES, embryonic stem; fEPSP, field excitatory postsynaptic potential; LTP, long-term potentiation; E-LTP, early LTP; L-LTP, late LTP; DNQX, 6,7-dinitroquinoxaline 2,3-dione; ACSF, artificial cerebrospinal fluid.

[c]T.D., M.K., and S.C. contributed equally to this work.

[j]R.Z., M.F., and P.M. contributed equally to this work.

[k]To whom correspondence should be addressed. E-mail: michael.frotscher@anat.uni-freiburg.de.

[l]To whom requests for materials should be addressed. E-mail: mundel@aecom.yu.edu.

www.pnas.org/cgi/doi/10.1073/pnas.1832384100

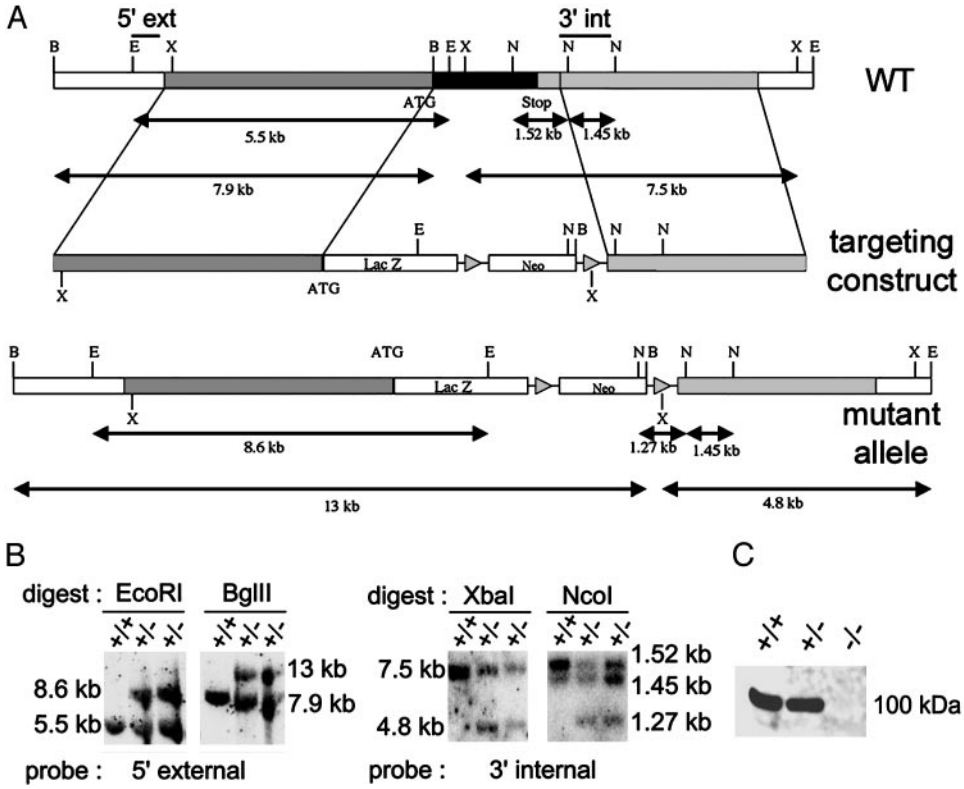

Fig. 1. Generation of *synaptopodin*-deficient mice. (*A*) Gene targeting strategy. The ORF of the *synaptopodin* gene (amino acids 2–690; black box) was replaced in frame by a *lacZ* cassette by using homologous recombination. (*B*) Southern blot analysis of genomic DNA from wild type (+/+) and two independent, heterozygous (+/−) ES cell clones. The correct recombination was determined by using a 5′ external probe on *Eco*RI/*Bgl*II digests and a 3′ internal probe on *Xba*I/*Nco*I digests, as well as Neomycin and LacZ probes (not shown). Both clones shown were used to generate chimeric mice. (*C*) Western blot analysis of cytosolic forebrain extracts prepared exactly as described (26) from (+/+), (+/−), and (−/−) mice by using the Synaptopodin-specific rabbit polyclonal antibody NT (26). The 100-kDa band corresponding to Synaptopodin was strongly expressed in +/+ and weaker in +/− mice, but was absent from −/− mice.

CA1 and stratum radiatum and stratum lucidum of CA3) from wild-type (male; $n = 5$) and mutant (male; $n = 5$) mice, the percentage of spines with a spine apparatus was determined. A regular spine apparatus was considered to be present if at least two dense plates and at least one tubule of sER were detected in close apposition.

Spine Counts. Frontal sections (100 μm; right hemisphere) from wild-type ($n = 5$) and mutant ($n = 5$) mice were used for Golgi-impregnation taking advantage of a section impregnation procedure (30). Sections were coded and spines were counted on apical dendrites of layer 5 pyramidal cells in the somatosensory cortex (82 cells in wild type and 82 cells in the mutant) and on oblique dendrites of CA1 pyramidal cells (57 cells in wild type and 48 cells in the mutant). In layer 5 cortical pyramidal cells, spines were counted in three successive segments of 83 μm each, beginning with the dendritic portion originating from the soma. In CA1 pyramidal cells, all spines on individual oblique dendrites were counted and expressed as spines per μm. The same cells were used to determine the percentage of mushroom spines (spines with a head diameter more than twice that of the spine neck; ref. 19; wild type: $n = 5$ animals, 15 cells, 750 spines; mutant: $n = 5$ animals, 15 cells, 750 spines). Statistical analysis involved an ANOVA for repeated measures and the Mann–Whitney *U* test. All spine counts were performed blind to genotype.

Spine Length. Spine length was measured on the same CA1 dendrites that were used for spine counting (wild type, $n = 5$; mutant, $n = 5$). A commercially available image analysis software (Analysis, SIS, Münster, Germany) was used to determine the length of all spines located within a single horizontal focus plane of the microscope. Five to eight dendrites per animal were analyzed. Between 32 and 162 spines were measured per dendrite (total number of spines measured: 6,495). The average length of spines as well as the distribution of spines within 0.25-μm-length categories were determined. The same cells were used to measure the length of mushroom spines (wild type: $n = 5$ animals, 15 cells, 750 spines; mutant: $n = 5$ animals, 15 cells, 750 spines). Statistical analysis was performed by using a nonparametric test (*U* test). All measurements were performed blind to genotype.

Electrophysiology. Hippocampal transverse slices (400 μm) were prepared as described elsewhere (31). Field excitatory postsynaptic potentials (fEPSP) measured in the CA1 stratum radiatum were evoked by stimulation of the Schaffer collateral-commissural afferents. Baseline recording of 20 min preceded application of high frequency stimulus. Long-term potentiation (LTP) was induced by three consecutive theta burst stimuli (TBS; 10 × 4 pulses with 200-ms interburst intervals and 10-ms intervals within each pulse) or tetani (three series of 30 pulses for a pulse length of 100 μs, 200 Hz). Poststimulation recordings continued for 80 min for early LTP (E-LTP) and 180 min for late LTP (L-LTP). For L-LTP measurements 180 min after stimulation, only slices that showed E-LTP were included in the analysis. Paired pulse recordings were done at intervals of 10, 20, 40, 80, and 160 ms after the initial pulse. Ensemble averages >6 were constructed by using all data points, aligned with respect to the time of LTP induction. LTP was counted as "successful" if there was an enhancement of the fEPSP slope to >120% of baseline average 55–60 min after TBS or tetanus application. All

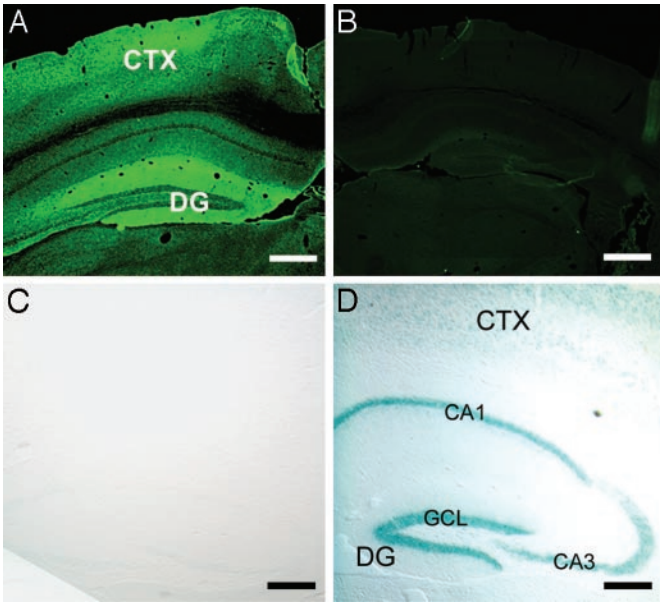

Fig. 2. Distribution of Synaptopodin protein and transcripts. (*A*) Immunofluorescence microscopy shows the expression of Synaptopodin in wild-type neocortex (CTX) and hippocampus. Note that immunolabeling is strongest in the dendritic layers (27, 28), particularly in those of the dentate gyrus (DG). (*B*) Absence of immunofluorescence in the mutant confirms the specificity of Synaptopodin immunolabeling and the successful deletion of the *synaptopodin* gene. (*C*) Absence of β-galactosidase activity in wild type. (*D*) *Synaptopodin* mRNA is expressed in the granule cell layer (GCL) of the dentate gyrus (DG), pyramidal cell layer of hippocampal areas CA3 and CA1 (27, 28), and in various layers of the neocortex (CTX) as shown by β-galactosidase activity in the mutant. (Scale bars: 400 μm.)

results were statistically analyzed by a Student's *t* test (two sided). To analyze the functionality of the *N*-methyl-D-aspartate (NMDA) receptor, fEPSPs were recorded in the following sequence: after 15 min baseline recording, 6,7-dinitroquinoxaline 2,3-dione (DNQX, 10 μM) in low Mg^{2+} (0.5 mM) artificial cerebrospinal fluid (ACSF) was applied via the bath. After 15 min DL-2-amino-5-phosphonovalerate (50 μM) together with DNQX were applied for 20 min to the same slice in low Mg^{2+} ACSF; afterward, normal ACSF was used for washout.

Behavioral Testing. Adult male wild-type ($n = 16$) and mutant mice ($n = 14$) were used. For the open field (100 × 60 × 30 cm, floor divided into squares, 10 × 10 cm each), mice were placed on the central square and the numbers of line crossings, rearings, and leanings were noted (15 min). The elevated plus maze consisted of a wooden apparatus with four arms of 40 × 10 cm at right angles, connected by a central platform 10 × 10 cm. Two of the opposed arms were enclosed by 40-cm-high walls (closed arms), whereas the other two arms had no walls (open arms). The whole apparatus was elevated 83 cm above the floor. Mice were placed on the central platform facing a closed arm and were allowed to freely explore (15 min). Because of the elevation, anxious animals preferentially enter closed arms. Entries into open and closed arms and the cumulative time spent on either type of arm were measured. The radial arm maze consisted of a central octogonal platform with eight regularly arranged Plexiglas arms (25 × 6 × 6 cm) with a hidden food pellet (10 mg) at the end of each arm. Extra-maze cues were present in the room. Animals were food-deprived to 85–90% of pretest body weight. Initially, two habituation trials (one per day; 15 min, free access to all arms) and a training period of 5 consecutive days (one trial per day) were performed. These were terminated after 15 min or after all eight rewards had been eaten. Repeated entries into one arm, time spent to eat all rewards, and number of novel entries within the first eight entries were all counted and scored (32).

Results

Lack of Spine Apparatuses in *synaptopodin*-Deficient Mice. The intronless ORF of the murine *synaptopodin* gene was targeted by homologous recombination in ES cells as shown in Fig. 1 *A* and *B*. Loss of the Synaptopodin protein in homozygous mutant mice was determined by Western blot analysis of adult forebrain tissue (Fig. 1*C*) and by immunostaining (Fig. 2 *A* and *B*). Activity for β-galactosidase was found in hippocampal principal neurons (Fig. 2 *C* and *D*), similar to the expression of synaptopodin mRNA (27). *Synaptopodin*-deficient mice (−/−) are viable and fertile in a mixed 129/C57BL6 genetic background and indistinguishable from wild-type (+/+) littermates under standard laboratory conditions. In particular, the fine structure and function of kidney podocytes, which express large amounts of Synaptopodin (26), are normal in mutant mice as judged by electron microscopy and urinary protein excretion analysis (S.C., K.S., B. Kränzlin, N. Gretz, W. Kriz, and P.M., unpublished observations). Standard neuroanatomical techniques revealed a normal cytoarchitecture of mutant brains. In addition, Golgi impregnation showed a normal shape, orientation, and dendritic arborization of single Golgi-impregnated neurons.

Electron microscopic analysis of Synaptopodin immunogold labeling revealed selective staining of the spine apparatus in wild-type animals (Fig. 3*A*), which prompted us to study this organelle in *synaptopodin*-deficient mice. In these mutants, we were unable to find spine apparatuses in spines of telencephalic neurons (Fig. 3*B*). In serial thin sections, only occasional sER cisterns were observed, lacking the electron-dense plates defining a spine apparatus. Blind quantitative analysis (Fig. 3*C*) of >15,000 spines in neocortex, striatum, and hippocampus of wild-type (+/+; $n = 5$) and mutant mice (−/−; $n = 5$) confirmed the loss of spine apparatuses in *synaptopodin*-deficient telencephalic neurons. However, the loss of spine apparatuses in mutant telencephalic neurons was not paralleled by a loss of spines. Spine counts in defined dendritic segments of Golgi-impregnated pyramidal cells in layer 5 of the neocortex and in CA1 pyramidal neurons did not reveal significant differences between wild-type ($n = 5$) and mutant ($n = 5$) mice (Fig. 3*D*). Because mushroom spines regularly contain a spine apparatus (19), we tested whether the loss of the spine apparatus could have selectively affected this spine subpopulation (Fig. 3*E*). However, no difference was observed between the percentage of mushroom spines in wild-type (17.2%) and mutant mice (17.33%). Similarly, measurements of spine length did not reveal differences in average spine length (Fig. 3*F*; wild type: 0.78 μm, mutant: 0.8 μm), differences in length categories (Fig. 3*G*), or mushroom spine length (Fig. 3*H*; wild type: 1.09 μm; mutant: 1.04 μm) between spines of wild-type animals and mutants. Analysis of serial thin sections through specialized spines, the large complex spines or excrescences on proximal dendrites of CA3 pyramidal cells known to contain a spine apparatus in wild type (33), showed that these spines were present as normal but lacked spine apparatuses. Interestingly, wild-type Purkinje cells in the cerebellum do not express Synaptopodin (26), and the spines of these neurons do not form a distinct spine apparatus and contain only occasional cisterns of sER (34).

LTP Is Impaired in *synaptopodin*-Deficient Mice. Because of the potential role of the spine apparatus and Synaptopodin in synaptic plasticity (35, 36), we analyzed LTP in hippocampal slices from adult wild-type and mutant mice (31). First, basal synaptic transmission was examined by comparing the size of the presynaptic fiber volley (PSFV; proportional to the number of presynaptic neurons recruited by stimulation) to the slope of the fEPSP. We found basal synaptic transmission to be normal in *synaptopodin*-deficient mice

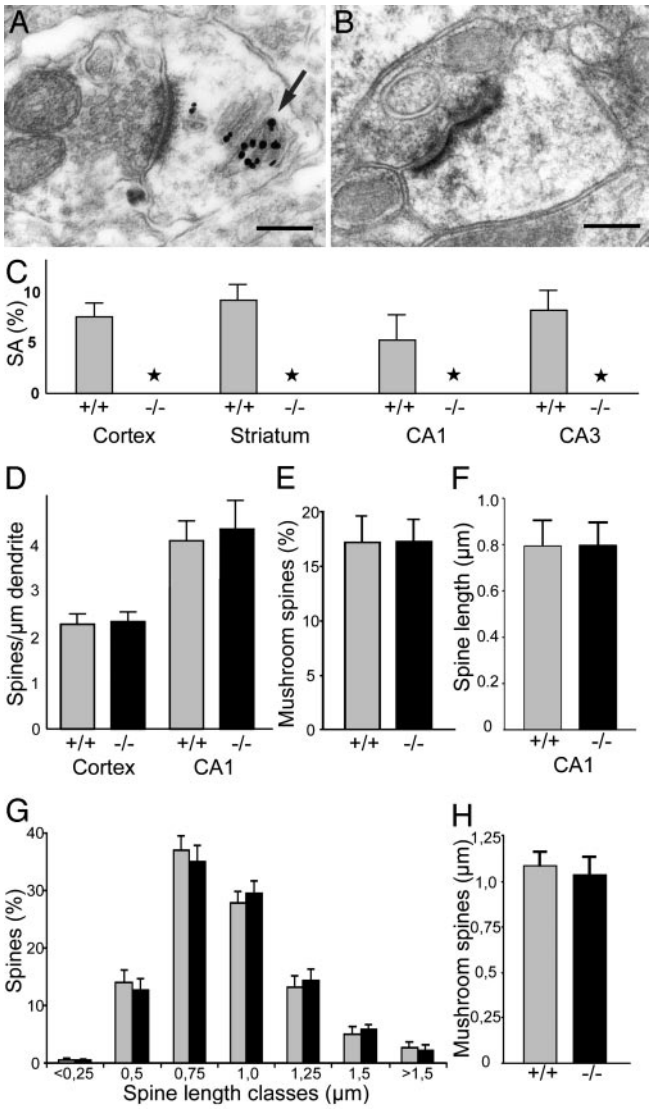

Fig. 3. *Synaptopodin*-deficient mice lack a spine apparatus. (*A*) Spine apparatus (arrow) in a wild-type hippocampal neuron; immunolabeled for Synaptopodin protein (1.4 nm gold grains, silver-intensified). (Scale bar: 0.2 μm.) (*B*) Absence of spine apparatus (and of Synaptopodin protein) in a hippocampal neuron from a *synaptopodin*-deficient mouse. (Scale bar: 0.2 μm.) (*C*) Average percentage (plus SD) of spines with a spine apparatus (SA) in wild-type (+/+) animals ($n = 5$) and *synaptopodin*-deficient (−/−) mice ($n = 5$). Number of spines analyzed (+/+ versus −/−): cortex (2,396/1,889), striatum (2,218/1,985), hippocampal area CA1 (2,488/2,218), hippocampal area CA3 (1,742/1,635). In *synaptopodin*-deficient mice (asterisks), the spine apparatus is absent in all regions analyzed. (*D*) The number of spines (plus SEM) on apical dendrites of Golgi-impregnated layer 5 pyramidal neurons and on dendrites of CA1 pyramidal neurons is similar in wild-type (+/+; $n = 5$) and *synaptopodin*-deficient (−/−; $n = 5$) mice. (*E*) The percentage of mushroom spines (plus SD) is comparable in wild type (+/+; $n = 5$) and *synaptopodin*-deficient mice (−/−; $n = 5$). (*F*) The length of spines (plus SD) was measured on dendrites of CA1 pyramidal neurons. No significant difference was observed between wild-type (+/+; $n = 5$) and *synaptopodin*-deficient (−/−; $n = 5$) mice. (*G*) Analysis of spine length classes (each class: 0.25 μm; plus SD) revealed a comparable distribution of spines in wild-type (+/+; $n = 5$) and *synaptopodin*-deficient (−/−; $n = 5$) mice. (*H*) The selective analysis of mushroom spine length (plus SD) did not show a significant difference between wild-type (+/+; $n = 5$) and *synaptopodin*-deficient (−/−; $n = 5$) mice.

(ratio EPSP slope/PSFV: mutant: $2.5 \pm 0.4, n = 32$; wild type: 2.4 ± 0.29; $n = 43$, $P > 0.1$, t test, two sided). In addition, paired-pulse facilitation was measured by applying two stimuli (separated by intervals ranging from 10 to 160 ms; Fig. 4*A*) and recording the evoked fEPSP. Again, no significant differences were seen comparing wild type to mutant mice for all tested intervals (Fig. 4*A*; $P > 0.1$). These results indicate that presynaptic function is normal in mutant mice. In contrast, LTP experiments revealed striking differences between wild-type and mutant mice: all *synaptopodin*-deficient mice tested showed a significantly reduced induction rate of E-LTP for both tetanus (Fig. 4*B*) and TBS protocols (Fig. 4 *C*, *E*, and *F*). For tetanic stimulation, the induction rate of LTP was significantly lower in mutant (47%) than wild-type mice (72%; Fig. 4*B*). For TBS, a similar reduction of LTP induction was observed (42% in mutant and 79% in wild-type mice; Fig. 4*C*). One hour after the LTP-inducing stimulus, mutant mice still displayed lower average slope values ($121 \pm 4.1\%$ compared with wild-type controls: $140 \pm 4.0\%$: Fig. 4*B*). In the TBS studies, mutant mice displayed an average slope of $118 \pm 4.8\%$, compared with $145 \pm 7.8\%$ in wild-type controls (Fig. 4*C*). In summary, both TBS- and tetanus-induced LTP are significantly reduced ($P < 0.01$) in *synaptopodin*-deficient adult mice. Three hours after stimulation, LTP is still clearly impaired in mutant mice ($111 \pm 7.7\%$, compared with $135 \pm 7.9\%$ in wild-type controls, $P < 0.05$; Fig. 4*D*). In summary, these experiments indicate that both the early as well as the late phase of LTP are disrupted in *synaptopodin*-deficient mice.

To assure that the observed defect was not trivially explained by a loss of NMDA receptors in the mutant animals, we tested α-amino-3-hydroxy-5-methyl-4-isoxazole-proprionate (AMPA) and NMDA receptor components of the fEPSP. In the presence of the AMPA receptor antagonist DNQX, slices from mutant mice showed a NMDA receptor component of the fEPSP comparable to control mice: in the wild-type mice, application of 10 μM DNQX (low Mg^{2+} ACSF) reduced the fEPSP slope to 22.5% ($\pm 2.2\%$) and 20.7% ($\pm 1.7\%$) in the *synaptopodin*-deficient mice ($P = 0.34$; Mann–Whitney test). In addition, when we added 50 μM DL-2-amino-5-phosphonovalerate, the responses were reduced to zero, indicating that the remaining responses after DNQX under low Mg^{2+} conditions were indeed NMDA receptor-mediated currents (Fig. 6, which is published as supporting information on the PNAS web site, www.pnas.org). This indicates that NMDA receptor function was normal in *synaptopodin*-deficient mice.

***Synaptopodin*-Deficient Mice Show Behavioral Deficits.** The impairment in the proposed cellular correlate of spatial learning in rodents, hippocampal CA3-CA1 LTP, prompted us to also analyze the behavioral phenotype in *synaptopodin*-deficient mice (Fig. 5). Would the absence of the spine apparatus have any effect on the behavioral level? First, locomotor activity was monitored by using the open field test. Although vertical activity (rearing and leaning) was normal (data not shown), *synaptopodin*-deficient mice displayed a decrease in their horizontal activity (Fig. 5*A*). Next, the mice were challenged by the elevated plus maze, which assesses their anxiety. Compared with wild-type controls, *synaptopodin*-deficient mice are less anxious (Fig. 5 *B–D*). Finally, spatial learning was analyzed by using the radial arm maze. To avoid anxiety-related effects, this spatial learning paradigm was chosen rather than the Morris water maze. *Synaptopodin*-deficient mice are impaired in their spatial learning ability as indicated by a significantly increased error rate ($P < 0.05$) in the radial arm maze during the last 3 days of training (Fig. 5*E*). The differences between genotypes were most pronounced on the fifth day of training, with the *synaptopodin*-deficient animals making twice as many errors as wild-type controls ($P < 0.01$).

Discussion

Our genetic analysis of Synaptopodin revealed an essential molecular function of this protein in the formation of spine apparatuses in spines of telencephalic neurons. The complete lack of spine apparatuses in the telencephalon of *synaptopodin*-deficient mice is paralleled by impaired synaptic plasticity. In

NEUROSCIENCE

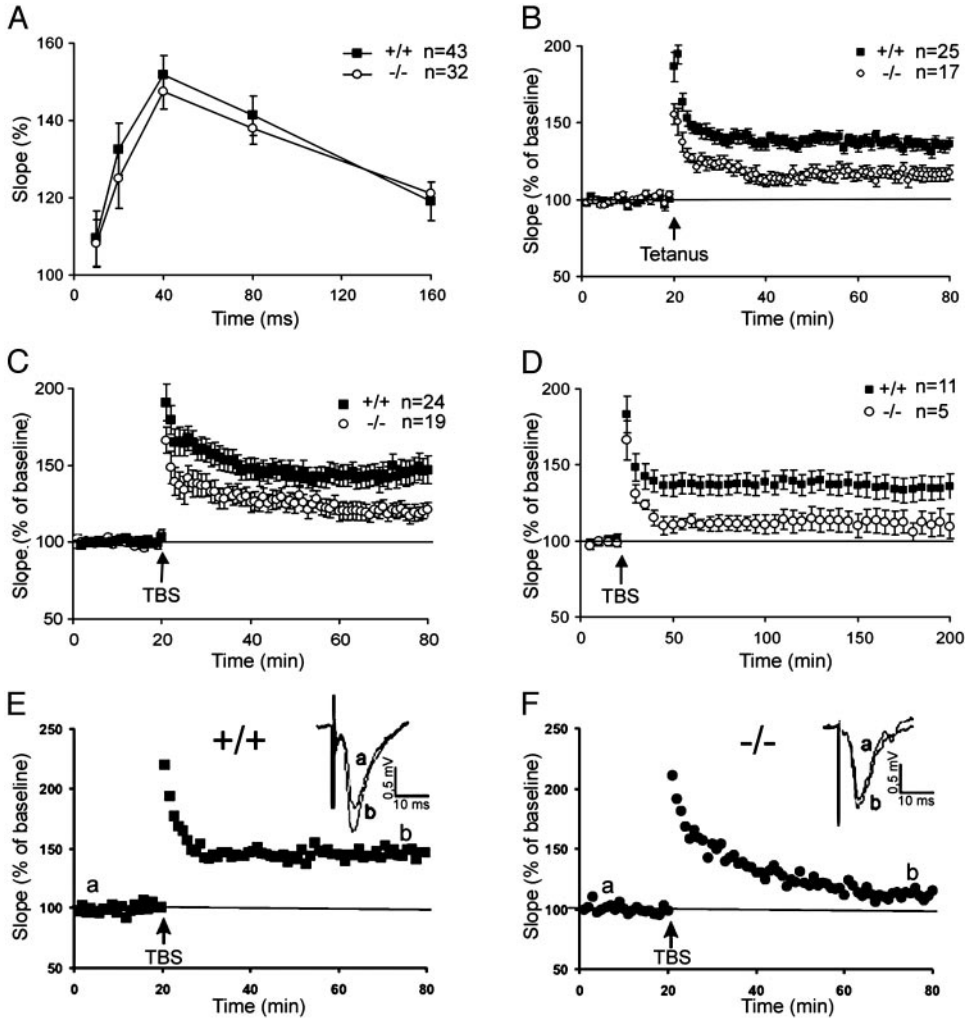

Fig. 4. Reduced LTP in the hippocampus of *synaptopodin*-deficient mice. (*A*) Paired-pulse facilitation (PPF) was not significantly different between mutant and wild-type mice. The percentages denote the ratio of the second EPSP slope size to the first EPSP slope. PPF was tested for 10-, 20-, 40-, 80-, and 160-ms interstimulus intervals (ISI). (*B*) Group data for fEPSP recordings before and after tetanus (100 Hz) application. The difference between *synaptopodin* mutant and wild-type mice is significant ($P < 0.01$). Error bars, SEM; *n*, number of slices. (*C*) Group data for fEPSP recordings before and after theta burst (TBS; 100 Hz) application. Also for TBS application the difference between mutant and wild-type mice is significant ($P < 0.01$; *t* test, two-sided). Error bars, SEM; *n*, number of slices. (*D*) Group data for fEPSP recordings before and 3 h after TBS (100 Hz) application. L-LTP is also affected in *synaptopodin*-deficient mice. The difference between mutant and wild-type mice is significant ($P < 0.05$; *t* test). Error bars, SEM; *n*, number of slices. Only slices that showed E-LTP were included in the analysis. (*E* and *F*) Single experiment for a wild-type mouse (*E*) and a *synaptopodin*-deficient animal (*F*). Arrow, application of TBS (100 Hz). Sample fEPSP traces before and after TBS application are displayed in *Insets*. Small letters next to the curve in the main graph indicate the time points at which the sample responses were taken.

particular, the absence of spine apparatuses is accompanied by a loss of LTP at Schaffer collateral synapses and by spatial learning impairments in *synaptopodin*-deficient mice. The present genetic analysis reveals a molecular link of the spine apparatus to synaptic plasticity and learning.

The spine apparatus consists of two structural elements, stacks of sER and electron-dense plates (18, 34). Of these two components, the formation of the electron-dense plates is likely to depend on *synaptopodin* expression, because they were absent in the mutants. Their absence may prevent the formation of narrow, parallel stacks of sER that were not observed in *synaptopodin*-deficient mice. However, the formation of sER in general does not seem to be disturbed, because it was regularly found in the perinuclear cytoplasm as well as in some spines and dendrites of *synaptopodin*-deficient mice. In this context, it is noteworthy that Synaptopodin is not expressed in the cerebellum (26). Although Purkinje cell spines contain sER, they lack the electron-dense plates and, accordingly, do not contain a regular spine apparatus (18, 34) (and interestingly also do not show LTP although they do show long-term depression). These studies indicate that the spine apparatus is a characteristic structure in spines of forebrain neurons and that the formation of its electron-dense plates and parallel stacks of sER must require Synaptopodin. The forced expression of Synaptopodin in Purkinje cells is a potential future way to further elucidate the role of Synaptopodin and the function of the spine apparatus.

Consisting of portions of sER, the spine apparatus is regarded as a calcium store (20, 21, 23) that may be involved in calcium-dependent mechanisms of synaptic function and plasticity. Furthermore, the spine apparatus seems to be linked to NMDA receptors (37) via a cytoskeletal bridge of actin and α-actinin-2 (38) and may be involved in NMDA receptor-mediated release of calcium from internal stores (24). In addition, the spine apparatus may modify local calcium decay kinetics within a spine, because calcium could be sequestered into its stacks of sER (3). Calcium influx through NMDA receptors, calcium-induced calcium release from internal stores, and calcium decay kinetics within the spine microcompartment are critically in-

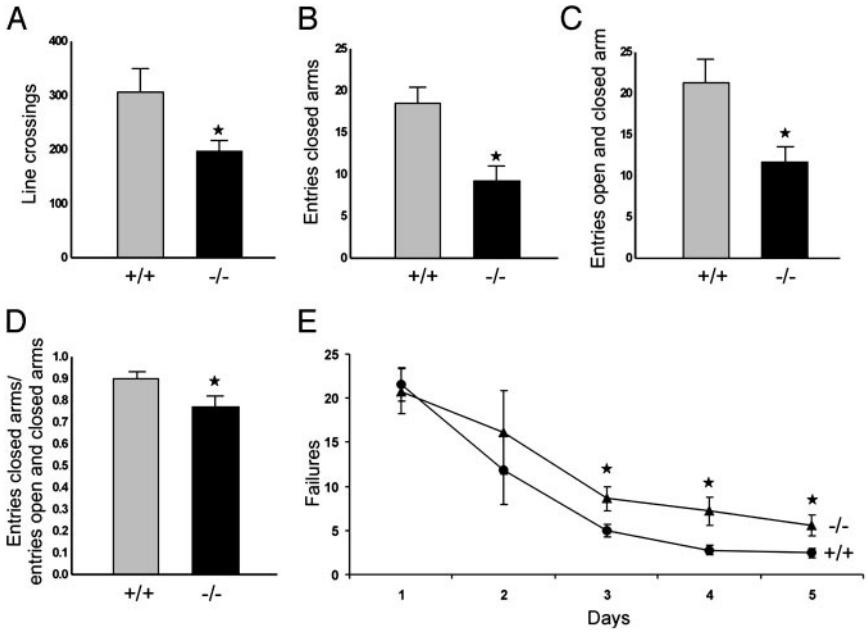

Fig. 5. Learning defects in *synaptopodin*-deficient mice. (*A*) Locomotor activity in the open field. Bars indicate mean numbers (+SEM) of line crossings. Mutant mice ($n = 9$) show less locomotor activity than wild-type controls ($n = 10$). (*B–D*) Anxiety-related behavior in the elevated plus maze. Frequency of closed (*B*) and all (*C*) arm entries (mean + SEM). The ratio of entries into closed arms versus all arms is illustrated in *D*. Note that mutant mice ($n = 9$) are less anxious than wild-type controls ($n = 10$), and that this difference is not caused by reduced locomotor activity. (*E*) Spatial learning in the radial arm maze. Mean numbers (±SEM) of spatial working memory errors of wild-type ($n = 16$; dots) and mutant ($n = 14$; triangles) mice during the 5-day training period. From day three on, mutant mice show significantly more failures than wild-type mice (*, $P < 0.05$).

volved in mechanisms of synaptic plasticity resulting in functional and structural changes at the synapses concerned (39, 40). Because only a subpopulation of ≈20% of the spines, typically the mushroom-shaped ones, have a spine apparatus in the adult (19), one might hypothesize that synapses containing a spine apparatus may be primarily involved in processes of synaptic plasticity. In the present study, we establish that LTP at Schaffer collateral synapses is reduced in *synaptopodin*-deficient mice. Future experiments will elucidate whether LTP at other synapses (mossy fiber synapses), and other forms of synaptic plasticity (long-term depression), are also affected in this mutant.

We thank M. Higuchi and K. Kaestner for vector cassettes. We are grateful to Kristina Vintersten for production of the chimeras. Furthermore, we thank H. Goedemans, C. Hofmann, T. Heider, A. Schneider, V. Staiger, and M. Winter for technical assistance, A. Hunziker for DNA sequencing, and R. Dono for comments on the manuscript. This work was supported by Deutsche Forschungsgemeinschaft Grants SFB 505 (to M.F.), SFB 269 (to T.D.), Mu1118/4-1 (to P.M. and R.Z.), and Graduiertenkolleg "Experimentelle Nieren- und Kreislaufforschung" (to A.Z.), the VW-Stiftung (to T.D., M.K., M.F., and T.B.), National Institutes of Health Grant DK 57683 (to P.M.), and the Max Planck Society (M.K. and T.B.). K.S. was supported by a fellowship from the Kidney and Urology Foundation of America.

1. Gray, E. G. (1959) *J. Anat.* **83,** 420–433.
2. Koch, C. & Zador, A. (1993) *J. Neurosci.* **13,** 413–422.
3. Majewska, A., Brown, E., Ross, J. & Yuste, R. (2000) *J. Neurosci.* **20,** 1722–1734.
4. Fischer, M., Kaech, S., Knutti, D. & Matus, A. (1998) *Neuron* **20,** 847–854.
5. Yuste, R. & Denk, W. (1995) *Nature* **375,** 682–684.
6. Engert, E. & Bonhoeffer, T. (1999) *Nature* **339,** 66–70.
7. Maletic-Savatic, M., Malinow, R. & Svoboda, K. (1999) *Science* **283,** 1923–1927.
8. Harris, K. M. & Kater, S. B. (1994) *Annu. Rev. Neurosci.* **17,** 341–371.
9. Fukazawa, Y., Saitoh, Y., Ozawa, F., Ohta, Y., Mizuno, K. & Inokuchi, K. (2003) *Neuron* **38,** 447–460.
10. Valverde, F. (1967) *Exp. Brain Res.* **3,** 337–352.
11. Frotscher, M., Hamori, J. & Wenzel, H. J. (1977) *Exp. Brain Res.* **30,** 549–560.
12. McKinney, R. A., Capogna, M., Dürr, R., Gähwiler, B. H. & Thompson, S. M. (1999) *Nat. Neurosci.* **2,** 44–49.
13. Woolley, C. S. & McEwen, B. S. (1993) *J. Comp. Neurol.* **336,** 293–306.
14. Murphy, D. D. & Segal, M. (1996) *J. Neurosci.* **16,** 4059–4068.
15. Buchs, P. A. & Muller, D. (2002) *Proc. Natl. Acad. Sci. USA* **96,** 8040–8045.
16. Muller, D., Toni, N. & Buchs, P. A. (2000) *Hippocampus* **10,** 596–604.
17. Harris, K. M. (1999) *Curr. Opin. Neurobiol.* **9,** 343–348.
18. Spacek, J. (1985) *Anat. Embryol.* **171,** 235–243.
19. Spacek, J. & Harris, K. M. (1997) *J. Neurosci.* **17,** 190–203.
20. Fifkova, E., Markham, J. A. & Delay, R. J. (1983) *Brain Res.* **266,** 163–168.
21. Svoboda, K. & Mainen, Z. F. (1999) *Neuron* **22,** 427–430.
22. Miller, S. G. & Kennedy, M. B. (1986) *Cell* **44,** 861–870.
23. Lisman, J. (1989) *Proc. Natl. Acad. Sci. USA* **86,** 9574–9578.
24. Emptage, N., Bliss, T. V. P. & Fine, A. (1999) *Neuron* **22,** 115–124.
25. Kovalchuk, Y., Eilers, J., Lisman, J. & Konnerth, A. (2000) *J. Neurosci.* **20,** 1791–1799.
26. Mundel, P., Heid, H. W., Mundel, T. M., Kruger, M., Reiser, J. & Kriz, W. (1997) *J. Cell Biol.* **139,** 193–204.
27. Deller, T., Merten, T., Roth, S. U., Mundel, P. & Frotscher, M. (2000) *J. Comp. Neurol.* **418,** 164–181.
28. Deller, T., Mundel, P. & Frotscher, M. (2000) *Hippocampus* **10,** 569–581.
29. Kaestner, K. H., Montoliu, L., Kern, H., Thulke, M. & Schütz, G. (1994) *Gene* **148,** 67–70.
30. Frotscher, M. (1992) *Microsc. Res. Tech.* **23,** 306–323.
31. Korte, M., Carroll, P., Wolf, E., Brem, G., Thoenen, H. & Bonhoeffer, T. (1995) *Proc. Natl. Acad. Sci. USA* **92,** 8856–8860.
32. Schwegler, H., Crusio, W. E. & Brust, I. (1990) *Neuroscience* **34,** 293–298.
33. Hamlyn, L. H. (1962) *J. Anat.* **97,** 112–120.
34. Peters, A., Palay, S. L. & Webster, H. (1991) *The Fine Structure of the Nervous System: Neurons and Their Supporting Cells* (Oxford Univ. Press, Oxford).
35. Yamazaki, M., Matsuo, R., Fukazawa, Y., Ozawa, F. & Inokuchi, K. (2001) *J. Neurochem.* **79,** 192–199.
36. Roth, S. U., Sommer, C., Mundel, P. & Kiessling, M. (2001) *Brain Pathol.* **11,** 169–181.
37. Racca, C., Stephenson, F. A., Streit, P., Roberts, J. D. & Somogyi, P. (2000) *J. Neurosci.* **20,** 2512–2522.
38. Wyszynski, M., Kharazia, V., Shanghvi, R., Rao, A., Beggs, A. H., Craig, A. M., Weinberg, R. & Sheng, M. (1999) *J. Neurosci.* **18,** 1388–1392.
39. Miyata, M., Finch, E. A., Khiroug, L., Hashimoto, K., Hayasaka, S., Oda, S. I., Inouye, M., Takagishi, Y., Augustine, G. J. & Kano, M. (2000) *Neuron* **28,** 233–244.
40. Sabatini, B. L., Oertner, T. G. & Svoboda, K. (2002) *Neuron* **33,** 439–452.